THE JOURNAL OF PHYSICAL CHEMISTRY Letters

Letter

pubs.acs.org/JPCL

Precise Identification of Graphene's Crystal Structures by Removable Nanowire Epitaxy

Jonghyeok Kim,[†,⊥] Kitaek Lim,[†,⊥] Yangjin Lee,[‡] Jongin Kim,[†] Kihwan Kim,[†] Jungwon Park,[*,§] Kwanpyo Kim,[*,‡] and Won Chul Lee[*,†]

[†]Department of Mechanical Engineering, Hanyang University, Ansan, Gyeonggi 15588, Republic of Korea

[‡]Department of Physics, Ulsan National Institute of Science and Technology (UNIST), Ulsan 44919, Republic of Korea

[§]School of Chemical and Biological Engineering, Seoul National University, Seoul 08826, Republic of Korea

Supporting Information

ABSTRACT: Monitoring crystallographic orientations of graphene is important for the reliable generation of graphene-based nanostructures such as van der Waals heterostructures and graphene nanoribbons because their physical properties are dependent on crystal structures. However, facile and precise identification of graphene's crystallographic orientations is still challenging because the majority of current tools rely on complex atomic-scale imaging. Here, we present an identification method for the crystal orientations and grain boundaries of graphene using the directional alignment between epitaxially grown AuCN nanowires and the underlying graphene. Because the nanowires are visible in scanning electron microscopy, crystal orientations of graphene can be inspected with simple procedures. Kernel density estimation that we used in analyzing the nanowire directions enables precise measurement of graphene's crystal orientations. We also confirm that the imaged nanowires can be simply removed without degrading graphene's quality, thus showing that the present method can be practically used for measuring graphene's crystal structures.

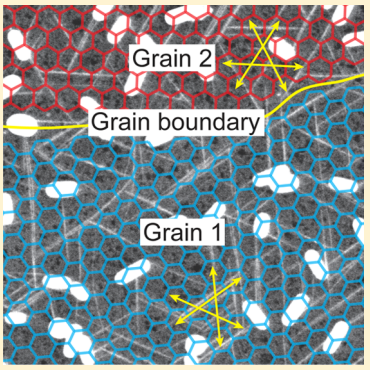

Graphene is a two-dimensional (2D) material that has been studied extensively over the last decades due to its unique and excellent physical properties. Recently, research efforts have been focused on fabricating nanoscale systems with graphene, for example, vertical stacking[1] of multiple graphene/2D material layers and nanoscale patterning[2] to produce desired lateral geometry of graphene. In these systems, controlling crystallographic orientations of graphene often enables the observation of unprecedented physical phenomena and the development of novel quantum electronic devices.[2−12] For example, a relative twist angle between the crystal lattices of graphene/2D material layers is a critical parameter that induces synergetic effects on electronic band structures[3−6] and resonant tunneling[7−10] in van der Waals heterostructures, and engineering crystallographic orientations of graphene nanoribbon edges[2,11] offers excellent control over electronic and spintronic properties. In addition, a tilt boundary from crystallographic misorientation between two lateral grains serves as one of the main sources of electrical and mechanical degradation of large-area polycrystalline graphene.[13] Therefore, an efficient measurement of crystallographic orientations and grain boundaries of graphene is strongly needed to facilitate investigation of intrinsic physical properties of graphene and its use in different types of devices.

Monitoring the crystal structures (crystallographic orientations and grain boundaries) of graphene has been attempted with different approaches, but efficient monitoring is still challenging. One of the fundamental reasons is that electrical and optical properties of single-crystalline graphene hardly show notable dependence on the crystal orientations.[14] This in-plain isotropic nature implies that inspecting graphene's crystal orientations based on electrical and optical measurements (in other words, macroscopic inspection without direct crystal imaging) is intrinsically difficult. Thus, atomic-scale investigation of graphene by transmission electron microscopy (TEM)[13,15] and scanning tunneling microscopy (STM)[16−18] has been a dominant approach, which enables the entire mapping of crystal structures of polycrystalline graphene. However, TEM can only scan a relatively small area (typically tens of micrometers) of samples that should be ultrathin for electron transparency.[13,15] These limitations make TEM-based investigation inefficient and incompatible with engineering procedures of graphene device fabrication. STM, another tool for atomic-resolution imaging, also has similar limitations because it requires ultraclean surfaces and time-consuming processes.[16−18] Alternatively, optical microscopy observing liquid crystals[19,20] or metal oxides[21,22] deposited onto graphene can be used to successfully investigate grain boundaries and/or relative misorientations between grains on a large scale (several hundred micrometers) with relatively simple procedures. However, the optical methods do not yield absolute crystallographic directions of grains in graphene, which

Received: February 4, 2017
Accepted: March 1, 2017
Published: March 1, 2017

DOI: 10.1021/acs.jpclett.7b00279
J. Phys. Chem. Lett. 2017, 8, 1302−1309

are essential for estimating and controlling of anisotropic characteristics of graphene-based nanoscale systems.

Recently, facile methods based on epitaxially grown nanomaterials (AuCN nanowires and MoS_2 nanotriangles) were suggested by our group[23] and other researchers,[24] and the methods enable us to measure crystal orientations and grain boundaries of graphene samples without relying on atomic-resolution measurements (Figure 1). It has been previously

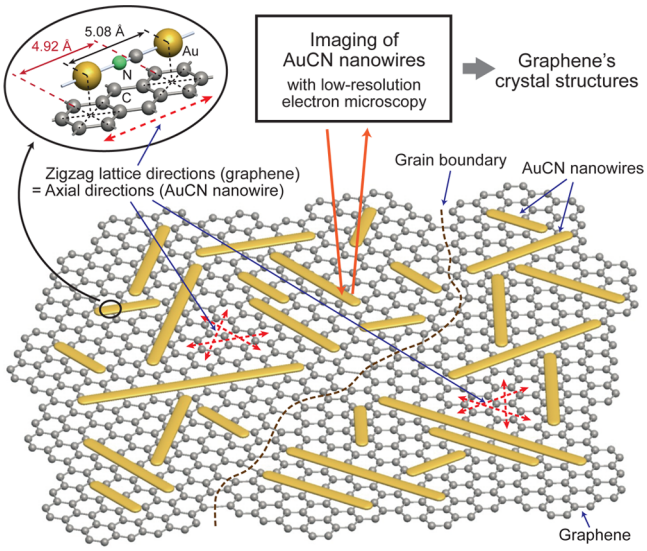

Figure 1. Schematic of the crystallographic mapping of graphene based on the epitaxial alignment of AuCN nanowires on graphene. Not only do the nanowire axes represent the zigzag lattice directions of graphene directly, but the changes in the nanowire axes directions also indicate tilt grain boundaries in the graphene. The inset shows a schematic view of the atomic configuration of AuCN aligned on graphene.

known that nanomaterials epitaxially grown on graphene (gold,[25,26] indium arsenide,[27−29] bismuth selenide,[30] phosphonic acid,[31] and molybdenum disulfide[32]) often align their outer morphologies along certain crystal orientations of the underlying graphene. Because the nanomaterial morphologies are large enough (about 10−100 nm scale) for visualization with scanning electron microscopy (SEM), recent methods[23,24] based on this epitaxial alignment can measure graphene's crystal structures with relatively simple procedures and are indeed compatible with microelectronics manufacturing techniques. The problem is, however, that the misalignment between the epitaxially grown nanomaterials and crystallographic orientations of the parent graphene substrate is unavoidable and often becomes severe due to the stochastic nature of nanomaterial nucleation on a surface. Although it is obvious that the misalignment between the nanomaterials and graphene compromises a measurement precision of graphene's crystal structures, this effect has not been considered in previous reports,[23,24] and quantitative attempts to calibrate the measurement are needed.

In this paper, we present an improved method for identifying graphene's crystal orientations and grain boundaries, which is robust to the epitaxial misalignment. Not only preserving an ability to measure crystal orientations and the simplicity in measurement procedures by using SEM visualization of AuCN nanowires epitaxially grown on graphene (Figure 1), the present method also increases the robustness by using a statistical technique of kernel density estimation. In order to evaluate the precision of the present method, we experimentally compared graphene's crystal orientations measured by the present method with those measured by TEM analysis. We also confirmed that we can identify graphene's grain boundaries by SEM imaging of AuCN nanowires and can remove the imaged nanowires by simple wet chemistry, thus showing that the present method can be practically used as a measurement tool for graphene's crystal structures.

In the experimental study, we used the axis directions of AuCN nanowires as visualization markers of the zigzag lattice directions of graphene (Figure 1). Our previous study[23] showed that the AuCN nanowires synthesized on graphene are preferentially oriented along the zigzag lattice directions of the graphene, because the lattice spacing (5.08 Å) of AuCN along the nanowire axis directions coincides well (lattice mismatch = 3.3%) with the length of two carbon hexagons (4.92 Å) along the graphene zigzag lattice directions. (Please check Supporting Information for details.) However, certain degrees of misalignments are unavoidable in practical samples; thus, the primary goal of this work is to evaluate how precisely crystal orientations of graphene can be measured from the AuCN nanowires. This evaluation requires not only images of AuCN nanowires on graphene but also reference values of the crystal orientations of the underlying graphene. Thus, we decided to use TEM for the evaluation because TEM can provide precise crystal structures of graphene with high magnification or electron diffraction as well as morphological images of AuCN nanowires with low magnification (similar to SEM's magnification). For the TEM analysis, we synthesized AuCN nanowires on suspended, single-layered graphene membranes in this study. We used two kinds of synthesis methods, as shown in Figure S1 and Supporting Methods. Both methods start from transferring CVD-synthesized graphene onto holey carbon TEM grids. In one of the methods, Au nanoparticles dispersed in organic solvents were drop-casted on the grids, and then, the grids were floated on an aqueous solution of 250 mM ammonium persulfate, $(NH_4)_2S_2O_8$, for 10 h. In the other method, an aqueous solution of 0.2 mM AuCN (dissolved in an ammonia solution) was simply dropped on the grid and dried for 15 min to synthesize the AuCN nanowires.

A typical TEM image of the prepared sample (Figure 2a) shows that horizontally grown AuCN nanowires are preferentially oriented along three directions on a graphene surface. We also captured a high-resolution TEM (HRTEM) image of the graphene in the same grain and measured graphene's crystal directions using two-dimensional FFT (fast Fourier transform) of the HRTEM image (Figure 2b). In Figure 2b, red dashed lines bisecting the angles between two neighboring spots (circled in yellow) represent the zigzag lattice directions of graphene in real lattice space. Thus, a direct comparison of panels a and b of Figure 2 confirms that the three directions of the nanowire axes have good rotational alignment to the zigzag lattice directions of the underlying graphene, as previously presented in our study.[23] This alignment is also confirmed statistically by a histogram of nanowire directions (Figure 2f), where the axial directions of the 63 nanowires in Figure 2a are distributed near the three orientations of graphene's zigzag lattices measured from Figure 2b.

While it is clear that a set of the nanowire directions can represent the zigzag lattice directions of graphene, whether an individual AuCN nanowire can precisely indicate graphene's lattice directions is questionable. We first checked this issue using atomic-resolution images of AuCN nanowires on graphene, which directly show both directions in a single image; the

DOI: 10.1021/acs.jpclett.7b00279
J. Phys. Chem. Lett. 2017, 8, 1302−1309

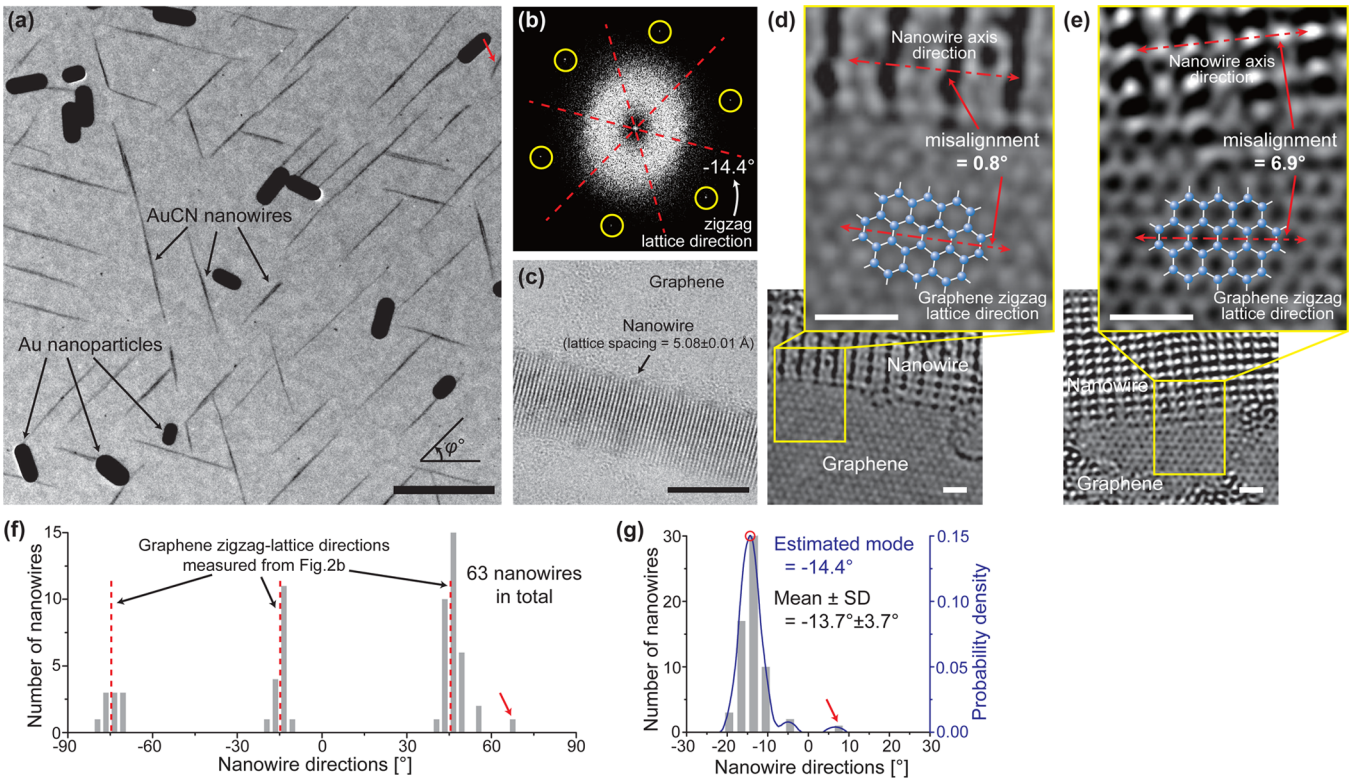

Figure 2. AuCN nanowires epitaxially aligned on graphene. (a) TEM image of the synthesized nanowires on graphene. The scale bar is 200 nm. (b) FFT image of the underlying graphene in (a). (c) HRTEM image of the synthesized nanowire on graphene. The scale bar is 10 nm. (d,e) Atomic-resolution TEM images of the synthesized nanowires on graphene. All scale bars are 0.7 nm. (f) Histogram of the angular distributions of the nanowire axes in (a). (g) Histogram (gray bars) and probability density function (blue line) constructed using the transformed angular directions of the nanowire axes in (a). The angular directions in (f) are transformed to be within ±30° based on the hexagonal symmetry of graphene. The probability density function is calculated using kernel density estimation.

Table 1. Summary of 10 Experiments Measuring the Crystal Orientations of Graphene by Using the Three Different Methods[a]

		graphene zigzag lattice direction	arithmetic mean of nanowire directions [deg]		kernel density estimation using nanowire directions [deg]	
figure #	number of nanowires [ea]	from FFT [deg] (standard measurement)	mean ± SD	error	estimated mode	error
Figure 2	63	−14.4	−13.7 ± 3.7	0.7	−14.4	0.0
Figure S2	105	−29.9	28.9 ± 5.4[b]	1.2[b]	29.9	0.2
Figure S3	155	−11.0	−10.2 ± 6.6	0.8	−11.6	0.6
Figure S4	33	24.1	19.8 ± 13.1	4.3	24.6	0.5
Figure S5	30	18.0	16.6 ± 5.9	1.4	17.8	0.2
Figure S6	28	−6.4	−7.4 ± 3.7	1.0	−6.4	0.0
Figure S7	12	−6.2	−6.5 ± 11.6	0.4	−6.0	0.2
Figure S8	18	−20.2	−13.9 ± 14.0	6.3	−20.0	0.2
Figure S9	18	26.4	25.0 ± 6.4[c]	1.4[c]	25.9	0.5
Figure S10	16	24.6	24.0 ± 2.1	0.6	24.8	0.2
rms (root-mean-square) of errors [deg]				2.6[d]		0.3

[a]The FFTs of HRTEM images are used as standard measurements, and the conventional (arithmetic mean) and present (kernel density estimation) methods are compared with the standards. [b]We obtain these values by transforming the nanowire orientations to a different angular range ($0° \le \theta < 60°$), as explained in Figure S2. The values based on the original range ($-30° \le \theta < 30°$) show an exceptionally large error of 25.8° (mean ± SD = 4.3 ± 26.5°) . [c]We obtain these values by transforming the nanowire orientations to a different angular range ($0° \le \theta < 60°$), as explained in Figure S9. The values based on the original range ($-30° \le \theta < 30°$) show a large error of 4.8° (mean ± SD = 21.6 ± 14.1°). [d]The rms error is 8.7° when the two original values (b,c) are used.

nanowire axis direction reasonably represents graphene's crystal direction in one sample (Figure 2d), but the other sample has a too large misalignment of 6.9° (Figure 2e). We analyzed the issue more statistically and quantitatively using the data set from Figure 2a,b. On the basis of the hexagonal symmetry of graphene, we transformed the nanowire axis directions to be in between −30° and 30° and drew a histogram of the transformed nanowire directions in Figure 2g. The large standard deviation of 3.7° indicates that the axis direction of an individual nanowire cannot robustly represent the zigzag lattice direction of graphene.

From the above results, one can simply expect that an arithmetic mean of nanowire axis directions (−13.7° in Figure 2g) can be a good measure of graphene's zigzag lattice orientation (−14.4° in Figure 2b), but interestingly, we found

DOI: 10.1021/acs.jpclett.7b00279
J. Phys. Chem. Lett. 2017, 8, 1302−1309

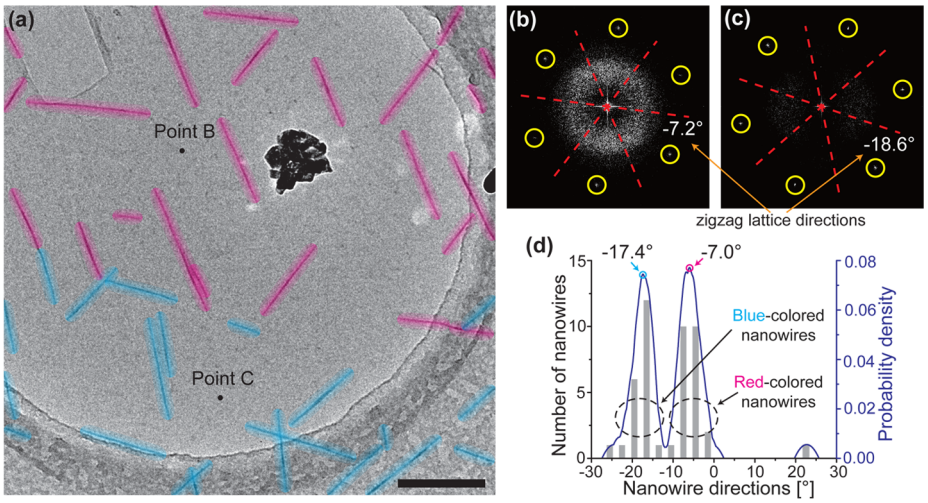

Figure 3. Using the AuCN nanowires to identify two neighboring grains with relatively tilted lattice directions in polycrystalline graphene. (a) Pseudocolored TEM image of the AuCN nanowires on graphene. The scale bar is 200 nm. (b,c) FFT images of graphene respectively captured at points B and C in (a). (d) Histogram (gray bars) and probability density function (blue line) constructed using the axial directions of the nanowires in (a).

that the arithmetic mean often misestimates graphene's crystal directions in other samples. We performed nine sets of additional experiments using three samples (Figures S2−S10), and the results are summarized in Table 1 (including the results from Figure 2). In each experiment, we performed the same analysis as that shown in Figure 2; we calculated the arithmetic mean of nanowire axis directions and compared it with graphene's zigzag lattice direction measured from FFT peaks. The difference between the two values can represent a measurement error of the arithmetic mean as a measure of graphene's zigzag lattice directions. The errors of the 10 measurements include exceptionally large values (Figures S4 and S8), and the rms (root-mean-square) error of 10 measurements is also too large (2.6°) for the precise measurement of graphene's crystal directions. Please note that a precision of <2° is necessary (a precision of ∼0.5° is recommended) for the crystallographic alignment between two layers of graphene or graphene/hBN in the van der Waals heterostructures[6,8,10] mentioned in the introductory section.

The major reason why the measurement errors in the arithmetic mean are larger than the general expectation is that a set of measured nanowire directions frequently contains outliers (largely misaligned nanowires). The outliers in the nanowire axis directions (marked as red arrows in Figure 2a,f,g) cause the arithmetic mean to have a biased value in favor of the outliers. In our 10 experiments, the outliers in the nanowire directions are almost unavoidable and even frequent; Figure S10 is the only result that contains no outlier, and Figure S4 shows that 3 nanowires are largely misaligned among 33 nanowires. This large misalignment can be due to the strong stochastic nature of surface reactions, defects in graphene molecular structures, and wrinkles in graphene membranes; thus, almost all heteroepitaxial growth of nanomaterials has the same problem. Because the optimization of synthesis conditions may be unable to remove such a stochastic phenomenon easily, this problem can be severe for precise measurement of graphene's crystal directions.

Thus, this work presents a precise measure of graphene's crystal orientation obtained from the nanowire axis directions based on kernel density estimation,[33−35] a technique in nonparametric statistics. In the present method, we estimate a probability density function (the blue curve in Figure 2g) from a measured set of the nanowire axis directions and calculate the angle at which the estimated probability density function has its maximum value (the angle at the peak, the red circled point in Figure 2g). In detail, the estimated probability density function, $f_p(\theta)$, is calculated using kernel density estimation[33−35] as follows

$$f_p(\theta) = \frac{I_{[-30°,30°)}(\theta)}{Nh} \sum_{i=1}^{N} \left\{ K\left(\frac{\theta - \theta_i}{h}\right) + K\left(\frac{\theta - \theta_i - 60°}{h}\right) + K\left(\frac{\theta - \theta_i + 60°}{h}\right) \right\}$$

where N is the total number of nanowires, θ_i is the transformed angular direction of the ith nanowire, $K(\theta)$ is an Epanechnikov kernel (one of the most optimal kernels),[33,36] h is the bandwidth of the kernel, and $I_A(\theta)$ is an indicator function. The angle at which $f_p(\theta)$ has its global or local maximum value is our new measure of graphene's zigzag lattice direction. (Please check Figure S11 and Supporting Methods for more details.) The statistical meaning of this method is to estimate a mode of a data set of the nanowire axis directions. Because a mode is insensitive to outliers compared to an arithmetic mean, the present method provides us a precise measure of graphene's zigzag lattice directions robust to large misalignments in nanowire axis directions. In all 10 measurements in our study (Table 1), the new measure delivers precise values whose errors are much reduced (all of the errors are less than 1°). Please also note that the measurement error does not increase even when the number of nanowires in the analysis is small (10−20 nanowires). The rms error in the crystal direction measurement based on kernel density estimation from the 10 experiments is obtained as 0.3°, which is 11.5% of the rms error (2.6°) using the arithmetic mean.

In addition, the present method has a practical advantage in angular calculation compared to the arithmetic mean. In the method based on the arithmetic mean, a calculation artifact can generate a large error when the zigzag lattice orientation of graphene is close to the upper or lower end of the angular range (±30° in this work). It is because, while the transformed nanowire direction of −30° equals 30° under the hexagonal symmetry of graphene, their effects are opposite in the

DOI: 10.1021/acs.jpclett.7b00279
J. Phys. Chem. Lett. 2017, 8, 1302−1309

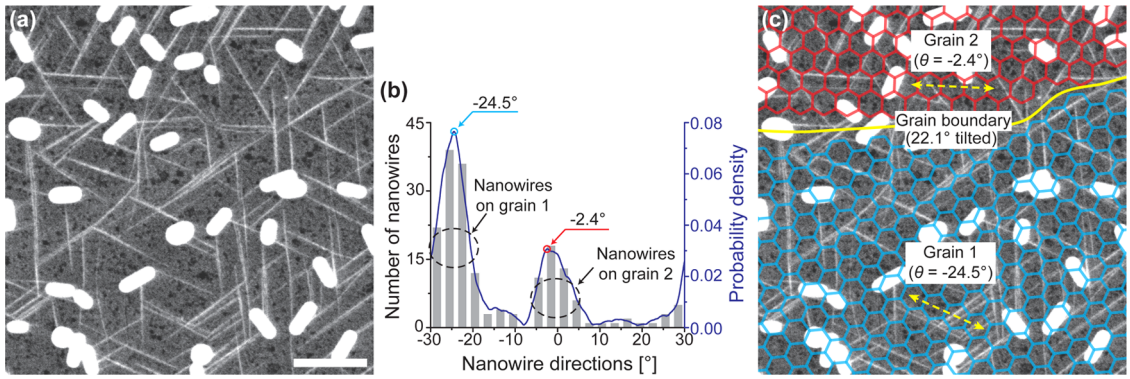

Figure 4. SEM-based visualization of the crystal orientations and grain boundaries of graphene. (a) SEM image of the synthesized nanowires on graphene. The scale bar is 200 nm. (b) Histogram (gray bars) and probability density function (blue line) constructed using the axial directions of the nanowires in (a). (c) The SEM image of (a) is shown with an overlay of the pseudolattice structures of graphene. The red and blue color maps represent different grains with relatively tilted lattice directions.

calculation of the arithmetic mean (Figures S2c and S9c). In this work, we removed this artifact by a simple method of transforming nanowire axis directions to angles between 0 and 60° (Figures S2d and S9d, Table 1), but a mathematically correct solution is to use an unfamiliar method, directional statistics.[37] The present method, however, can easily remove the calculation artifact near ±30° by defining kernel functions as connected at the two ends of −30 and 30° (Figure S11). As a result, the present method delivers the same value of directions even when different angular ranges are used (Figures S2c,d and S9c,d).

The present method is also effective to analyze two neighboring grains that are tilted from one to the other. Figure 3a shows a TEM image of AuCN nanowires on a graphene membrane that has a tilt grain boundary. The two different FFTs (Figure 3b,c), respectively obtained at points B and C in Figure 3a, confirm two grains in the underlying graphene and indicate their zigzag lattice directions (−7.2 and −18.6°). We measured the nanowire axis directions from Figure 3a and obtained a probability density function (Figure 3d) using the kernel density estimation. Two major peaks in the probability density function clearly indicate two graphene grains that are tilted with each other, and the two angles at the local maxima (−7.0 and −17.4°) measure graphene's zigzag lattice directions precisely (the errors are 0.2 and 1.2°, respectively). The present method can also visualize the two grains in graphene as shown in Figure 3a (presented by red and blue shadows). The angle (−12.6°) at the local minimum in Figure 3d enables us to classify the nanowires into two groups whose transformed axis directions are smaller (red) and larger (blue) than the angle. One remaining issue in Figure 3 is that the exact position of the grain boundary is unclear due to the low density of nanowires, and we will further discuss this issue in the next part.

While we performed all of the above experimental analyses using TEM (in order to measure the reference values of graphene's lattice orientations), the main purpose of the present method is to measure graphene's crystal directions and grain boundaries using SEM. Figure 4 shows that the present method can achieve this main purpose. Field-emission SEM enables us to visualize AuCN nanowires on graphene (please note that the graphene was transferred on a SiO_2-coated silicon wafer) with acceptable magnification (Figure 4a). A probability density function (Figure 4b) based on the present method indicates that the underlying graphene has two grains whose zigzag lattice directions are −2.4 and −24.5°. Although we cannot perform any reference measurement in this experimental setting, the analyses in the previous sections suggest that the measurement uncertainty of crystal directions in Figure 4 is less than ∼1°. Please also note that the tilt grain boundary of graphene is relatively clear in Figure 4 due to the high areal density of AuCN nanowires. A pseudocolored image in Figure 4c summarizes all of the information measured by the present method, including the crystal orientations of graphene grains, the tilt angle of the grain boundary, and the position of the grain boundary.

The primary output of the present measurement method is crystal orientations of grains in graphene, and we can identify grain boundaries by the changes in the crystal orientations. This indirect identification generates a limitation on detecting grain boundaries, which are also crucial for controlling electrical and physical properties of graphene. The present method cannot identify grain boundaries whose tilt angles are small. In detail, if the change of the crystal directions of a certain grain boundary is smaller than the distribution of nanowire directions in one grain, the grain boundary cannot be detected and two grains are misidentified as a single grain. To prevent this misidentification, the two peaks must be distinguished from each other in the probability density function estimated by the present method (such as Figures 3d and 4b). Thus, the fwhm (full width at half-maximum) of the peaks in the probability density functions indicates that the present method has a minimum detectable tilt angle of ∼7°. A solution to overcome this detection limit might be combining the present method with previous methods[38−40] suggesting the decoration and identification of grain boundaries. Because both the present and previous methods utilize nanomaterial deposition followed by SEM visualization, they can be easily combined without additional processes. The combined method may be able to provide entire mapping of crystal directions and grain boundaries in graphene with SEM.

We also note that AuCN nanowires used in this study can be synthesized and removed easily by using simple wet processes, thus enhancing advantages of using AuCN nanowries as a marker material. Other inorganic nanomaterials that can grow on graphene heteroepitaxially (gold,[25,26] indium arsenide,[27−29] bismuth selenide,[30] and molybdenum disulfide[32]) are synthesized using CVD (chemical vapor deposition) or evaporation, and high temperature (>600 °C) during or after synthesis is essential for heteroepitaxial alignment. (Please note that organic molecules can be heteroepitaxially aligned to graphene in ambient conditions, but they are invisible with SEM.) These harsh conditions for the synthesis may damage graphene and/or other materials in analysis targets, while AuCN nanowires used in

DOI: 10.1021/acs.jpclett.7b00279
J. Phys. Chem. Lett. 2017, 8, 1302−1309

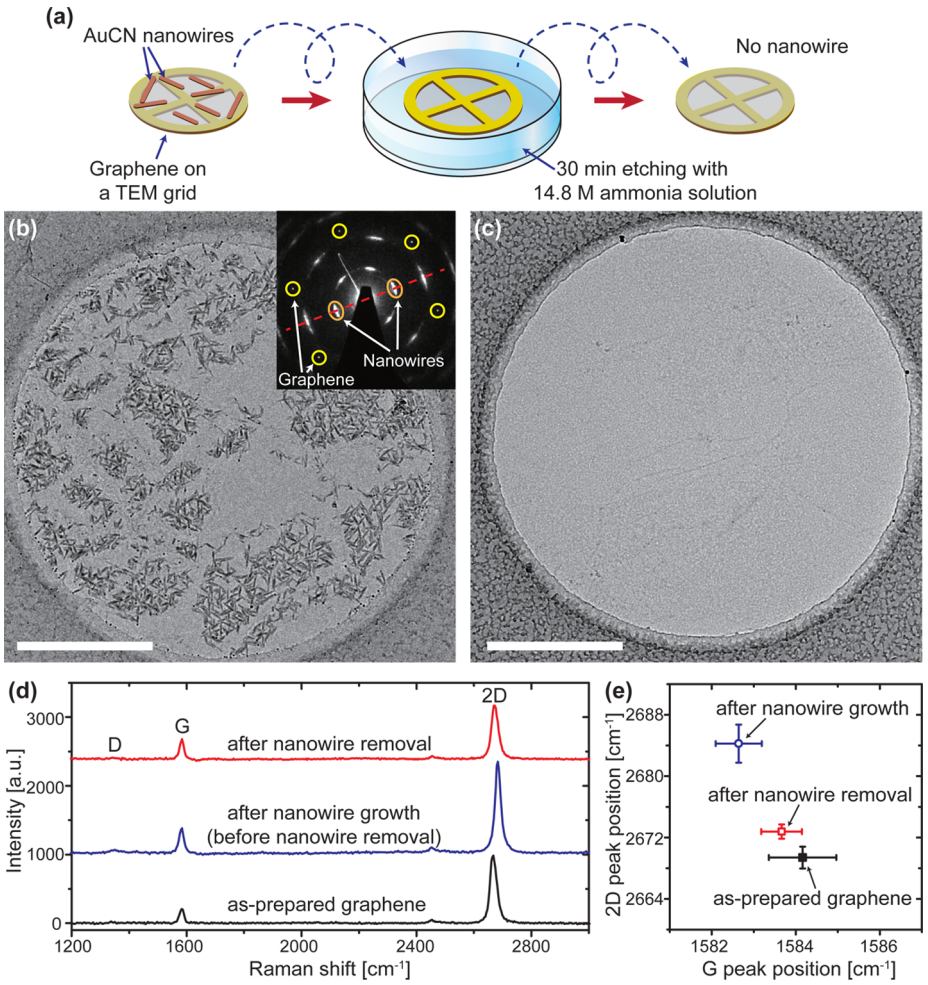

Figure 5. Removal of AuCN nanowires using a simple wet chemistry. (a) Schematic view of the removal process. (b,c) TEM images of the nanowire−graphene sample before (b) and after (c) removing AuCN nanowires. The scale bars are 500 nm. The inset in (b) shows an electron diffraction pattern of the nanowire−graphene sample. (d) Raman spectrum of pristine graphene (black), that after nanowire growth (blue), and that after nanowire removal (red). (e) Comparison of graphene Raman G and 2D peak positions. The error bars indicate standard deviations obtained from five samples.

this study are synthesized using aqueous solution at room temperature. In addition to the mild synthesis conditions, the simple removal is also an important factor as marker materials. As mentioned in the previous study, grain structure visualization using MoS_2 has a limited application area because the removal of MoS_2 on graphene is difficult.[24] However, AuCN nanowires in this work can be easily removed from graphene substrates using a 14.8 M ammonia solution (Figure 5). The Raman spectra of graphene before and after nanowire etching (Figure 5d) maintain very low D peaks, confirming that measurable defects are not generated in the underlying graphene during the synthesis and removal processes of AuCN nanowires. The graphene after nanowire synthesis shows shifts in G and 2D peak positions compared to as-prepared samples (Figure 5e), indicating the change in doping and possibly strain of graphene via interaction with AuCN.[41,42] On the other hand, G and 2D peaks mostly recover their original positions after nanowire removal. These observations from the Raman spectra imply that the AuCN nanowires can be synthesized and removed without degrading graphene's qualities and properties. Thus, the simplicity in the synthesis and removal of AuCN nanowires provides not only facile analysis of graphene's crystal structures but also the ability to use the graphene after the analysis.

In conclusion, we have presented a precise and facile method for identifying crystal directions and grain boundaries of graphene. The present method based on SEM imaging of AuCN nanowires and kernel density estimation enables the crystallographic analysis of graphene robust to the unavoidable misalignment between the nanowires and graphene. The concept and analysis method the we have introduced here can be applied to crystallographic mapping of other types of 2D materials using other types of epitaxially grown nanomaterials, thus broadening application areas of the present method.

■ ASSOCIATED CONTENT

Supporting Information

The Supporting Information is available free of charge on the ACS Publications website at DOI: 10.1021/acs.jpclett.7b00279.

Details of sample preparation, experimental procedures, and analysis methods of nanowire directions and plots of crystal direction measurements of graphene using AuCN nanowires (PDF)

■ AUTHOR INFORMATION

Corresponding Authors

*E-mail: jungwonpark@snu.ac.kr (J.P.).

DOI: 10.1021/acs.jpclett.7b00279
J. Phys. Chem. Lett. 2017, 8, 1302−1309

*E-mail: kpkim@unist.ac.kr (Kwanpyo K.).
*E-mail: wonchullee@hanyang.ac.kr (W.C.L.).

ORCID

Jungwon Park: 0000-0003-2927-4331
Kwanpyo Kim: 0000-0001-8497-2330
Won Chul Lee: 0000-0001-8479-0836

Author Contributions

⊥Jonghyeok K. and K.L. contributed equally to this work.

Notes

The authors declare no competing financial interest.

■ ACKNOWLEDGMENTS

This work was supported by the Basic Science Research Program and the Convergence Technology Development Program for Bionic Arm through the National Research Foundation of Korea (NRF) funded by the Ministry of Science, ICT & Future Planning (2016R1C1B1014940 and 2015M3C1B2052811). Y.L. and Kwanpyo K. gratefully acknowledge support from the Basic Science Research Program through the National Research Foundation of Korea (NRF) funded by the Ministry of Education (NRF-2016R1D1A1B03934008). Work at the Molecular Foundry was supported by the Office of Science, Office of Basic Energy Sciences, of the U.S. Department of Energy under Contract No. DE-AC02-05CH11231.

■ REFERENCES

(1) Novoselov, K. S.; Mishchenko, A.; Carvalho, A.; Castro Neto, A. H. 2D Materials and van der Waals Heterostructures. *Science* **2016**, *353* (6298), 461−474.
(2) Magda, G. Z.; Jin, X. Z.; Hagymasi, I.; Vancso, P.; Osvath, Z.; Nemes-Incze, P.; Hwang, C. Y.; Biro, L. P.; Tapaszto, L. Room-Temperature Magnetic Order on Zigzag Edges of Narrow Graphene Nanoribbons. *Nature* **2014**, *514* (7524), 608−611.
(3) Ponomarenko, L. A.; Gorbachev, R. V.; Yu, G. L.; Elias, D. C.; Jalil, R.; Patel, A. A.; Mishchenko, A.; Mayorov, A. S.; Woods, C. R.; Wallbank, J. R.; Mucha-Kruczynski, M.; Piot, B. A.; Potemski, M.; Grigorieva, I. V.; Novoselov, K. S.; Guinea, F.; Fal'ko, V. I.; Geim, A. K. Cloning of Dirac Fermions in Graphene Superlattices. *Nature* **2013**, *497* (7451), 594−597.
(4) Dean, C. R.; Wang, L.; Maher, P.; Forsythe, C.; Ghahari, F.; Gao, Y.; Katoch, J.; Ishigami, M.; Moon, P.; Koshino, M.; Taniguchi, T.; Watanabe, K.; Shepard, K. L.; Hone, J.; Kim, P. Hofstadter's Butterfly and the Fractal Quantum Hall Effect in Moire Superlattices. *Nature* **2013**, *497* (7451), 598−602.
(5) Hunt, B.; Sanchez-Yamagishi, J. D.; Young, A. F.; Yankowitz, M.; LeRoy, B. J.; Watanabe, K.; Taniguchi, T.; Moon, P.; Koshino, M.; Jarillo-Herrero, P.; Ashoori, R. C. Massive Dirac Fermions and Hofstadter Butterfly in a van der Waals Heterostructure. *Science* **2013**, *340* (6139), 1427−1430.
(6) Lee, M.; Wallbank, J. R.; Gallagher, P.; Watanabe, K.; Taniguchi, T.; Falko, V. I.; Goldhaber-Gordon, D. Ballistic Miniband Conduction in a Graphene Superlattice. *Science* **2016**, *353* (6307), 1526−1529.
(7) Britnell, L.; Gorbachev, R. V.; Geim, A. K.; Ponomarenko, L. A.; Mishchenko, A.; Greenaway, M. T.; Fromhold, T. M.; Novoselov, K. S.; Eaves, L. Resonant Tunnelling and Negative Differential Conductance in Graphene Transistors. *Nat. Commun.* **2013**, *4*, 1794.
(8) Mishchenko, A.; Tu, J. S.; Cao, Y.; Gorbachev, R. V.; Wallbank, J. R.; Greenaway, M. T.; Morozov, V. E.; Morozov, S. V.; Zhu, M. J.; Wong, S. L.; Withers, F.; Woods, C. R.; Kim, Y. J.; Watanabe, K.; Taniguchi, T.; Vdovin, E. E.; Makarovsky, O.; Fromhold, T. M.; Fal'ko, V. I.; Geim, A. K.; Eaves, L.; Novoselov, K. S. Twist-Controlled Resonant Tunnelling in Graphene/Boron Nitride/Graphene Heterostructures. *Nat. Nanotechnol.* **2014**, *9* (10), 808−813.
(9) Fallahazad, B.; Lee, K.; Kang, S.; Xue, J. M.; Larentis, S.; Corbet, C.; Kim, K.; Movva, H. C. P.; Taniguchi, T.; Watanabe, K.; Register, L. F.; Banerjee, S. K.; Tutuc, E. Gate-Tunable Resonant Tunneling in Double Bilayer Graphene Heterostructures. *Nano Lett.* **2015**, *15* (1), 428−433.
(10) Wallbank, J. R.; Ghazaryan, D.; Misra, A.; Cao, Y.; Tu, J. S.; Piot, B. A.; Potemski, M.; Pezzini, S.; Wiedmann, S.; Zeitler, U.; Lane, T. L. M.; Morozov, S. V.; Greenaway, M. T.; Eaves, L.; Geim, A. K.; Fal'ko, V. I.; Novoselov, K. S.; Mishchenko, A. Tuning the Valley and Chiral Quantum State of Dirac Electrons in van der Waals Heterostructures. *Science* **2016**, *353* (6299), 575−579.
(11) Son, Y. W.; Cohen, M. L.; Louie, S. G. Half-Metallic Graphene Nanoribbons. *Nature* **2006**, *444* (7117), 347−349.
(12) Kim, K.; Coh, S.; Tan, L. Z.; Regan, W.; Yuk, J. M.; Chatterjee, E.; Crommie, M. F.; Cohen, M. L.; Louie, S. G.; Zettl, A. Raman Spectroscopy Study of Rotated Double-Layer Graphene: Misorientation-Angle Dependence of Electronic Structure. *Phys. Rev. Lett.* **2012**, *108* (24), 24613.
(13) Huang, P. Y.; Ruiz-Vargas, C. S.; van der Zande, A. M.; Whitney, W. S.; Levendorf, M. P.; Kevek, J. W.; Garg, S.; Alden, J. S.; Hustedt, C. J.; Zhu, Y.; Park, J.; McEuen, P. L.; Muller, D. A. Grains and Grain Boundaries in Single-Layer Graphene Atomic Patchwork Quilts. *Nature* **2011**, *469* (7330), 389−392.
(14) Castro Neto, A. H.; Guinea, F.; Peres, N. M.; Novoselov, K. S.; Geim, A. K. The Electronic Properties of Graphene. *Rev. Mod. Phys.* **2009**, *81* (1), 109.
(15) Kim, K.; Lee, Z.; Regan, W.; Kisielowski, C.; Crommie, M. F.; Zettl, A. Grain Boundary Mapping in Polycrystalline Graphene. *ACS Nano* **2011**, *5* (3), 2142−2146.
(16) Coraux, J.; N'Diaye, A. T.; Busse, C.; Michely, T. Structural Coherency of Graphene on Ir(111). *Nano Lett.* **2008**, *8* (2), 565−570.
(17) Varchon, F.; Mallet, P.; Magaud, L.; Veuillen, J. Y. Rotational Disorder in Few-Layer Graphene Films on 6*H*-SiC(000-1): A Scanning Tunneling Microscopy Study. *Phys. Rev. B: Condens. Matter Mater. Phys.* **2008**, *77* (16), 165415.
(18) Loginova, E.; Nie, S.; Thurmer, K.; Bartelt, N. C.; McCarty, K. F. Defects of Graphene on Ir(111): Rotational Domains and Ridges. *Phys. Rev. B: Condens. Matter Mater. Phys.* **2009**, *80* (8), 085430.
(19) Kim, D. W.; Kim, Y. H.; Jeong, H. S.; Jung, H. T. Direct Visualization of Large-Area Graphene Domains and Boundaries by Optical Birefringency. *Nat. Nanotechnol.* **2011**, *7* (1), 29−34.
(20) Son, J. H.; Baeck, S. J.; Park, M. H.; Lee, J. B.; Yang, C. W.; Song, J. K.; Zin, W. C.; Ahn, J. H. Detection of Graphene Domains and Defects Using Liquid Crystals. *Nat. Commun.* **2014**, *5*, 3438.
(21) Duong, D. L.; Han, G. H.; Lee, S. M.; Gunes, F.; Kim, E. S.; Kim, S. T.; Kim, H.; Ta, Q. H.; So, K. P.; Yoon, S. J.; Chae, S. J.; Jo, Y. W.; Park, M. H.; Chae, S. H.; Lim, S. C.; Choi, J. Y.; Lee, Y. H. Probing Graphene Grain Boundaries with Optical Microscopy. *Nature* **2012**, *490* (7419), 235−239.
(22) Yu, S. U.; Cho, Y.; Park, B.; Kim, N.; Youn, I. S.; Son, M.; Kim, J. K.; Choi, H. C.; Kim, K. S. Fast Benchtop Visualization of Graphene Grain Boundaries Using Adhesive Properties of Defects. *Chem. Commun.* **2013**, *49* (48), 5474−5476.
(23) Lee, W. C.; Kim, K.; Park, J.; Koo, J.; Jeong, H. Y.; Lee, H.; Weitz, D. A.; Zettl, A.; Takeuchi, S. Graphene-Templated Directional Growth of an Inorganic Nanowire. *Nat. Nanotechnol.* **2015**, *10* (5), 423−428.
(24) Ago, H.; Fukamachi, S.; Endo, H.; Solis-Fernandez, P.; Mohanad Yunus, R.; Uchida, Y.; Panchal, V.; Kazakova, O.; Tsuji, M. Visualization of Grain Structure and Boundaries of Polycrystalline Graphene and Two-Dimensional Materials by Epitaxial Growth of Transition Metal Dichalcogenides. *ACS Nano* **2016**, *10* (3), 3233−3240.
(25) Zhou, H. Q.; Yu, F.; Chen, M. J.; Qiu, C. Y.; Yang, H. C.; Wang, G.; Yu, T.; Sun, L. F. The Transformation of a Gold Film on Few-Layer Graphene to Produce Either Hexagonal or Triangular Nanoparticles During Annealing. *Carbon* **2013**, *52*, 379−387.
(26) Luo, Z. T.; Somers, L. A.; Dan, Y. P.; Ly, T.; Kybert, N. J.; Mele, E. J.; Johnson, A. T. C. Size-Selective Nanoparticle Growth on Few-Layer Graphene Films. *Nano Lett.* **2010**, *10* (3), 777−781.
(27) Hong, Y. J.; Yang, J. W.; Lee, W. H.; Ruoff, R. S.; Kim, K. S.; Fukui, T. van der Waals Epitaxial Double Heterostructure: InAs/Single-Layer Graphene/InAs. *Adv. Mater.* **2013**, *25* (47), 6847−6853.

DOI: 10.1021/acs.jpclett.7b00279
J. Phys. Chem. Lett. 2017, 8, 1302−1309

(28) Hong, Y. J.; Lee, W. H.; Wu, Y. P.; Ruoff, R. S.; Fukui, T. van der Waals Epitaxy of InAs Nanowires Vertically Aligned on Single-Layer Graphene. *Nano Lett.* **2012**, *12* (3), 1431−1436.
(29) Hong, Y. J.; Fukui, T. Controlled van der Waals Heteroepitaxy of InAs Nanowires on Carbon Honeycomb Lattices. *ACS Nano* **2011**, *5* (9), 7576−7584.
(30) Dang, W. H.; Peng, H. L.; Li, H.; Wang, P.; Liu, Z. F. Epitaxial Heterostructures of Ultrathin Topological Insulator Nanoplate and Graphene. *Nano Lett.* **2010**, *10* (8), 2870−2876.
(31) Prado, M. C.; Nascimento, R.; Moura, L. G.; Matos, M. J. S.; Mazzoni, M. S. C.; Cancado, L. G.; Chacham, H.; Neves, B. R. A. Two-Dimensional Molecular Crystals of Phosphonic Acids on Graphene. *ACS Nano* **2011**, *5* (1), 394−398.
(32) Shi, Y. M.; Zhou, W.; Lu, A. Y.; Fang, W. J.; Lee, Y. H.; Hsu, A. L.; Kim, S. M.; Kim, K. K.; Yang, H. Y.; Li, L. J.; Idrobo, J. C.; Kong, J. van der Waals Epitaxy of MoS_2 Layers Using Graphene as Growth Templates. *Nano Lett.* **2012**, *12* (6), 2784−2791.
(33) Silverman, B. W. *Density Estimation for Statistic and Data Analysis*; Chapman & Hall/CRC, 1986.
(34) Rosenblatt, M. Remarks on Some Nonparametric Estimates of a Density Function. *Ann. Math. Stat.* **1956**, *27* (3), 832−837.
(35) Parzen, E. On Estimation of a Probability Density Function and Mode. *Ann. Math. Stat.* **1962**, *33* (3), 1065−1076.
(36) Epanechnikov, V. A. Non-Parametric Estimation of a Multivariate Probability Density. *Theory Probab. Its Appl.* **1969**, *14* (1), 153−158.
(37) Fisher, N. I.; Lewis, T.; Embleton, B. J. J. *Statistical Analysis of Spherical Data*; Cambridge University Press, 1987.
(38) Wang, X. R.; Tabakman, S. M.; Dai, H. J. Atomic Layer Deposition of Metal Oxides on Pristine and Functionalized Graphene. *J. Am. Chem. Soc.* **2008**, *130* (26), 8152−8153.
(39) Kim, K.; Lee, H. B. R.; Johnson, R. W.; Tanskanen, J. T.; Liu, N.; Kim, M. G.; Pang, C.; Ahn, C.; Bent, S. F.; Bao, Z. Selective Metal Deposition at Graphene Line Defects by Atomic Layer Deposition. *Nat. Commun.* **2014**, *5*, 4781.
(40) Yu, S. U.; Park, B.; Cho, Y.; Hyun, S.; Kim, J. K.; Kim, K. S. Simultaneous Visualization of Graphene Grain Boundaries and Wrinkles with Structural Information by Gold Deposition. *ACS Nano* **2014**, *8* (8), 8662−8668.
(41) Das, A.; Pisana, S.; Chakraborty, B.; Piscanec, S.; Saha, S. K.; Waghmare, U. V.; Novoselov, K. S.; Krishnamurthy, H. R.; Geim, A. K.; Ferrari, A. C.; Sood, A. K. Monitoring Dopants by Raman Scattering in an Electrochemically Top-Gated Graphene Transistor. *Nat. Nanotechnol.* **2008**, *3* (4), 210−215.
(42) Lee, J. E.; Ahn, G.; Shim, J.; Lee, Y. S.; Ryu, S. Optical Separation of Mechanical Strain from Charge Doping in Graphene. *Nat. Commun.* **2012**, *3*, 1024.

DOI: 10.1021/acs.jpclett.7b00279
J. Phys. Chem. Lett. 2017, 8, 1302−1309